The Meteoritical Society

Meteoritics & Planetary Science 47, Nr 10, 1537–1557 (2012)
doi: 10.1111/j.1945-5100.2012.01417.x

Nonporphyritic chondrules from equilibrated Rumuruti and ordinary chondrites: Chemical evidence of secondary processing

Maria Eugenia VARELA[1*], Paul SYLVESTER[2], Almut ENGLER[3], and Gero KURAT[4†]

[1]Instituto de Ciencias Astronómicas de la Tierra y del Espacio (ICATE) Av. España 1512 sur, J5402DSP San Juan, Argentina
[2]Department of Earth Sciences, Memorial University of Newfoundland, St. John's NF A1B 3X5, Canada
[3]Department of Mineralogy and Petrology, University of Graz, Universitätsplatz 2, A8010 Graz, Austria
[4]Department of Lithospheric Sciences, University of Vienna, Althanstrasse 14, 1090 Vienna, Austria
[*]Corresponding author. E-mail: evarela@icate-conicet.gob.ar
[†]Deceased

(Received 03 May 2012; revision accepted 14 August 2012)

Abstract–Nineteen nonporphyritic pyroxene and pyroxene/olivine chondrules, chondrule fragments, and irregular objects were studied from two equilibrated chondrites, the ordinary (L/LL5) Knyahinya chondrite and the Rumuruti type (R4) Ouzina chondrite. Major element contents for almost all objects in the chondrites are disturbed from their chondritic ratios, most probably during metamorphic re-equilibration. However, the volatile elements (Na_2O + K_2O) in Ouzina scatter around the CI line, probably the result of being generated and/or processed in different environments as compared with those for Knyahinya. All studied objects from Knyahinya and Ouzina possess systematically fractionated trace element abundances. Depletion of LREE with respect to HREE and ultra-refractory HFSE documents variable degrees of LREE transport into an external mineral sink and restricted mobility of most of the HREE and HFSE. Moderately volatile elements preserve volatility-controlled abundances. Strongly fractionated Rb/Cs ratios (up to 10× CI) in all studied objects suggest restricted mobility of the large Cs ion. All studied objects sampled and preserved Y and Ho in solar proportions, a feature that they share with the nonporphyritic chondrules of unequilibrated ordinary chondrites.

INTRODUCTION

Chondrules are millimeter- to micrometer-sized spherical silicate objects that are the most abundant components of most chondritic meteorites (e.g., up to 75% by mass). These droplet-shaped objects, that have been at least partly liquid during the course of their histories (''fiery rain'' of Sorby 1877; ''droplet chondrule'' of Gooding and Keil 1981), preserved extreme compositional (chemical and isotopic) diversity.

Based on their textures, chondrules can be divided into two groups: porphyritic and nonporphyritic. Porphyritic chondrules consist mainly of olivine or pyroxene phenocrysts, or a mixture of both minerals, in a fine-grained or glassy silicate matrix, whereas the nonporphyritic ones have various textures, including granular olivine-pyroxene (GOP), radial pyroxene (RP), and crystocrystalline (C) (Gooding and Keil 1981). Barred-olivine (BO) chondrules are considered to be special kinds of porphyritic chondrules (e.g., Gooding and Keil 1981); however, they possess certain characteristics (e.g., platy textures indicating rapid crystallization from a liquid) that warrants their distinction from other porphyritic chondrules. Although researchers have studied chondrules for decades, much less attention has been paid by geochemists to nonporphyritic chondrules as compared with porphyritic ones.

This is a petrographic and chemical (major and minor trace element analyses) study of nonporphyritic-textured objects (e.g., pyroxene/olivine chondrules, chondrule fragments, irregular objects) and barred-olivine (BO) chondrules in two chondrites: Knyahinya

and Ouzina. Knyahinya is classified as an L/LL5 ordinary chondrite (e.g., Jarosewich 1990) and Ouzina is a Rumuruti type (R4) chondrite (Grossman 2000). All the common textural types of chondrules are observed in LL chondrites, but in R chondrites the nonporphyritic types are relatively rare (approximately 2–4%, e.g., Rubin 2010; Bischoff et al. 2011). R chondrites, Pecora Escarpment (PCA) 91002, and Acfer 217 are exceptions, where nonporphyritic chondrules constitute 10% and 8%, respectively (Kallemeyn et al. 1996), which is only slightly lower than their abundance in ordinary chondrites (approximately 15%, Gooding and Keil 1981).

The Van Schmus and Wood (1967) classification scheme for chondrites links the degree of chemical homogenization of the major silicates to the degree of recrystallization (e.g., metamorphism). Petrologic types 4–6, which comprise the equilibrated ordinary chondrites (EOCs), including Knyahinya, exhibit moderate (type 4) to strong (type 6) metamorphism, and corresponding alteration of their textural and chemical features.

In particular, enhanced solid-state diffusion of the major cations (Mg^{2+} and Fe^{2+}) at elevated temperatures has led to "equilibration" (homogenization) of the chemical compositions of the major minerals such as olivine and pyroxene in most equilibrated chondrites. In contrast, in type 3 or unequilibrated ordinary chondrites (UOCs), metamorphism and alteration are minor to negligible and pristine compositions are preserved, whereas in types 1 and 2 chondrites, aqueous alteration has occurred at low temperatures (approximately 100º C) (e.g., Scott 2007).

An estimate of the thermal conditions under which metamorphism took place in equilibrated chondrites can be made by studying chemical exchange between minerals. Based on Fe–Mg exchange between olivine and spinel, Kessel et al. (2007) found that the average equilibration temperatures (the lowest temperature for solid-state diffusion) for a suite of H, L, and LL ordinary chondrites of petrologic types 4–6, cover a narrow range between 586 and 777 °C as compared with previous determinations of metamorphic temperatures (e.g., < 600–950 °C, Heyse 1978). For R4-5 chondrites, olivine-chromite geothermometry indicates equilibration temperatures of 550–690 °C (Wlotzka 2005). Because secondary processes (e.g., thermal events) contribute to the modification of primary features, it is important to understand the relationship between the primary indicators of petrographic type (e.g., texture and chemical composition of phases) and the conditions under which formation and/or re-equilibration of elements could have taken place.

Here, petrographic and chemical (major and minor trace element analyses) data for silicate phases in nonporphyritic chondrules, chondrule fragments, and related objects in Knyahinya and Ouzina are examined to elucidate the extent to which chemical composition of these objects reflect primary as opposed to secondary processes. This evaluation is enhanced through comparison of the new data for Knyahinya and Ouzina with the chemical compositions of nonporphyritic chondrules from UOCs (Engler et al. 2007). The preserved geochemical characteristics of the studied objects can help to reveal differences between the environments in which Knyahinya and Ouzina were generated and/or processed.

Preliminary trace element patterns for some Knyahinya and Ouzina objects were published in Engler et al. (2004).

SAMPLES AND ANALYTICAL METHODS

Thirteen chondrules and other objects were analyzed in polished thin and thick sections in L/LL5 Knyahinya (from A763/B) and six objects in R4 Ouzina (N 2155). All samples belong to the Natural History Museum (NHM) in Vienna. Abbreviations of sample names used throughout this paper are as follows: KN = Knyahinya and OZ = Ouzina.

Analytical Techniques

Objects were selected for chemical analysis using an optical microscope and a scanning electron microscope. Major element chemical compositions were obtained with a JEOL 6400 analytical scanning electron microscope (ASEM) (NHM; Vienna) and a CAMECA SX100 electron microprobe (Department of Lithospheric Science, University of Vienna). Electron microprobe analyses (EMPA) were performed at 15 kV acceleration potential and 15 nA sample current. Natural and synthetic standards were used for calibration. Scan widths of approximately 7.5×10 μm were made over several nonoverlapping areas with total dimensions of 80×80 μm and averaged to give estimated bulk compositions. In addition, major element contents of silicate phases were measured by ASEM and EMPA using finer beam sizes. A problem with rastered beam analyses is that the ZAF corrections for the bulk composition may be different from those in the individual minerals present. This is probably a minor problem when only silicates, are involved, but can lead to errors when phases with greatly different densities, such as metal and sulfide, are present. While the latter phases occur in minor and trace amounts in the studied samples, the lack of corrections based on density differences (Warren 1997; Berlin et al. 2008) could reduce the accuracy of the bulk elemental contents.

The bulk trace element contents of the chondrules and other objects, as well as trace element contents of individual silicate phases within each object, were measured with a VG Plasma Quad II+ "S" ICPMS and a 266 nm Q-switched Nd-YAG laser at the Memorial University of Newfoundland (for a detailed description of the system see Jackson et al. 1992; Jenner et al. 1993; Jackson 2001). The laser was pulsed at a frequency of 10 Hz, with an energy of 0.3–0.4 mJ per pulse. The first 40 s of each measurement were acquired with the laser off to determine the background count rates for each analysis. The sample was then ablated for 50–80 s, depending on the stability of the acquired signals and the thickness of the mineral in the section. Ablation pit diameters ranged between 10 and 40 μm (usually 40 μm), depending on the area of interest and/or the object size. For bulk analyses of the objects, either a 100 x 100 μm box raster or 40 x 100 μm line scan was used, depending on the grain size and homogeneity of chondrules and fragments. Engler et al. (2007) presented the detailed conditions under which trace element analyses were performed, as well as a description of the standardization procedure and an estimate of the accuracy of the analytical method.

It should be kept in mind that in situ methods for obtaining bulk analyses of micro-objects in thin/thick sections using ASEM, EMPA, and LA-ICP-MS must assume that the volume analyzed is representative of the whole object, particularly as we are analyzing three dimensional objects with spots selected using two dimensional images of the sections. Although we tried to measure the true bulk value by making rasters or scans over representative areas, depending on the homogeneity and grain size of each individual object, the bulk analyses by ASEM, EPMA, and LA-ICP-MS should be considered as the best approximation that we could obtain for the actual bulk elemental contents.

RESULTS

Petrography

This study was focused on nonporphyritic chondrules, chondrule fragments, and related objects. The diameters of the analyzed objects range from about 180 μm to 2 mm. Shapes of objects vary between well rounded (spherical to ellipsoidal) and irregular. Based on these variations, the objects were divided into the following four groups (using the same nomenclature as in Engler et al. 2007): (i) chondrules (C); (ii) chondrule fragments (CF); (iii) irregular objects (IO), which have textures similar to those of chondrules but do not show any evidence of ever having been part of a spherical object; and (iv) unclassified objects (U), which are texturally and/or compositionally distinct from nonporphyritic chondrules, e.g., with crystals up to 80 μm or objects containing large amounts of metal and sulfide.

The dominant silicate phases of the different objects are olivine, low-Ca pyroxene, high-Ca pyroxene, and glass or devitrified glass. Plagioclase is subordinate. Metal and sulfides, which usually occur in minor to trace amounts inside the objects, are Ni-Fe (kamacite, taenite, with subordinate tetra-taenite) and troilite. Accessory phases are chromite and apatite. The principal petrographic characteristics of all studied objects are summarized in Table 1.

Major Textures

Most of the objects are nonporphyritic chondrules with mainly granular, fibrous, platy (fine and coarse), or subordinated dendritic textures (Table 1; Figs. 1a–e). In some objects, there are transitions between fibrous and granular textures (depending on the section plane, e.g., KN17), as well as fibrous and platy textures (depending on the size of the fibers/plates). In others, fibrous and granular-platy shapes are present (e.g., OZ4, OZ5; Figs. 1e–f).

A special feature occurs in KN3, as the barred olivine object contains a large apatite crystal enclosed by the olivine bars (Fig. 1c). In KN21 the core shows different composition and texture compared with the major part of the object. Coarse-grained metal and sulfides occur, as well as chromite and apatite, overgrown by the major part of the chondrule.

Chemical Composition of Individual Phases

Representative analyses are listed in Table 2. The results may be summarized as:

Olivine

Elemental abundances of olivine in objects of Knyahinya and Ouzina show a narrow range for major elements, with $Fo_{73–76}$ and $Fo_{60–61}$, respectively.

Low-Ca Pyroxene

There is almost no variation in the major element composition of low-Ca pyroxene in objects of the equilibrated chondrites, where pyroxenes with $En_{74.0–77.4}$ occur.

High-Ca Pyroxene

Augite-diopside occurs with a maximum wollastonite component of $Wo_{50.3}$. Titanium contents reach a maximum of 0.8 wt%, Cr_2O_3 and MnO contents are up to 1 and 0.7 wt%, respectively. Contents of Al_2O_3 differ

Table 1. Petrography of Knyahinya (L/LL5) and Ouzina (R4) objects.

Object	Shape	Diameter	Texture	Max. grain size	Surface features	Mineralogy	Annotations
KN1	IO irregular	1.3 mm	GPO (granular-fibrous)	< 10 μm	Irregular surface; thick ol-mantle	Low-Ca px, ol, glass, M/S	
KN2	IO irregular	300 μm	RPO-GPO (platy-fibrous and granular)	< 10 μm	Highly irregular surface	Low-Ca px, high-Ca px ol, plag, M/S	Object core: ol, px, plag (fibrous to fine-grained) object mantle: massy ol, glass
KN3	IO irregular	900 μm	BO + apatite (platy-ol)	50 μm	Irregular surface with M/S grains attached	Ol, glass, M/S ap, cr	Apatite inside the barred-olivine object
KN6	C spherical	800 μm	GPO (granular)	10 μm	Irregular surface	Low-Ca px, high-Ca px ol, plag, M/S	High-Ca px surrounds low-Ca px
KN7	IO irregular	850 μm	GPO (fibrous-granular)	30 μm, ol 60 μm	Highly irregular surface	Low-Ca px, ol, glass, M/S	Inhomogenous structure: zone with coarse-grained ol
KN8	C well rounded	600 μm	GP (granular)	10 μm	Irregular surface	Low-Ca px, high-Ca px glass, M/S	KN8 and KN9 stick together and have very similar textures
KN9	CF well rounded	500 μm	GP (granular)	10 μm	Irregular surface	Low-Ca px, high-Ca px glass, M/S	KN8 and KN9 stick together and have very similar textures
KN12	IO partly rounded	1.2 mm	RPO-GPO (fibrous-granular)	30 μm	Highly irregular surface	Low-Ca px, high-Ca px ol, glass, M/S	High-Ca px as rims of low-Ca px ol seems to be a secondary phase (due to Fe-enrichment?)
KN13	IO irregular	1.2 mm	GPO (fibrous)	10 μm	Irregular surface with some coarse M/S grains attached	Low-Ca px, ol, plag M/S, cr	
KN15	IO irregular	1 mm	BOP (platy-ol)	80 μm	Irregular surface	Low-Ca px, high-Ca px ol, plag, M/S, cr	Plag and high-Ca px form fine-grained crystals in between the ol and low-Ca px plates
KN16	C spherical -ellipsoidal	700 μm	GP (granular)	30 μm	Irregular surface	Low-Ca px, high-Ca px mes, M/S	High-Ca px as rims of low-Ca px, and as fine crystals in the mesostasis
KN17	CF ellipsoidal	1.4 mm	RP-GPO (platy-granular)	60 μm	Irregular surface with ol-mantle locally attached	Low-Ca px, high-Ca px ol, mes, M/S	Strongly inhomogeneous structure; high-Ca px as rims of low-Ca px, and as fine crystals in the mesostasis
KN21	C ellipsoidal	1 mm	GP (granular-platy)	30 μm	Irregular surface with some M/S grains attached	Low-Ca px, high-Ca px mes, M/S	Core has a different texure and coarse M/S, cr and ap crystals; high-Ca px as fine crystals in the mesostasis

Table 1. *Continued*. Petrography of Knyahinya (L/LL5) and Ouzina (R4) objects.

Object	Shape	Diameter	Texture	Max. grain size	Surface features	Mineralogy	Annotations
OZ1	U irregular	550 μm	ROP-BO (platy-ol)	10 μm	Highly irregular with a thick ol-mantle	High-Ca px, plag ol, cr	
OZ2	U irregular	400 μm	GOP (platy)	60 μm	Highly irregular with a thick ol-mantle	High-Ca px, plag ol, cr	
OZ4	CF irregular-partly rounded	650 μm	GOP (granular-platy)	50 μm	Irregular with ol-mantle	High-Ca px, plag ol, cr	
OZ5	IO irregular	180 μm	GPO (granular-fibrous)	< 10 μm	Irregular with coarse and strongly altered M/S grains attached	High-Ca px, plag ol, cr	
OZ6	U irregular	400 μm	GOP (granular-fibrous)	10 μm	Irregular surface	High-Ca px, plag ol, cr	Strongly inhomogeneous structure; large voids
OZ8	IO irregular	2 mm	BO (platy-ol)	80 μm	Irregular surface	High-Ca px, mes, ol, cr	Plag in mesostasis

ap = apatite; BO = barred olivine; BOP = barred-olivine pyroxene; C = chondrule; CF = chondrule fragment; cr = chromite; GP = granular pyroxene; GOP = granular olivine pyroxene; GPO = granular pyroxene object; IO = irregular object; M/S = metal/sulfide; mes = mesostasis; ol = olivine; px = pyroxene; plag = plagioclase; RP = radiating pyroxene; RPO = radial pyroxene object; U = unclassified object.

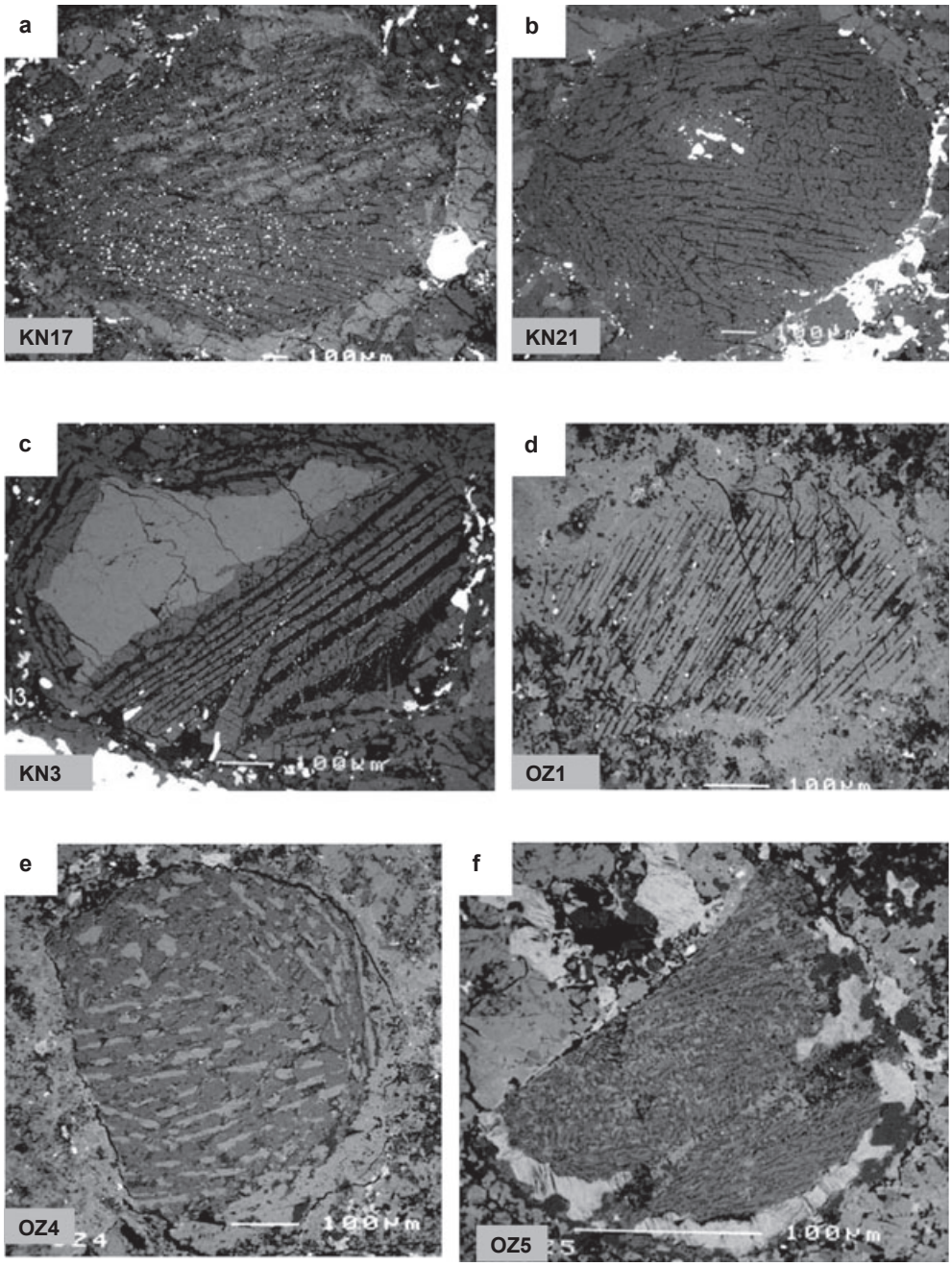

Fig. 1. Backscattered electron images of objects with a) radial pyroxene and platy-granular texture (KN17), scale: 100 μm; b) platy-granular texture (KN21). The core differs in texture and composition from the major object, scale: 100 μm; c) barred olivine with coarse platy texture (KN3) with a large apatite, scale: 100 μm; d) radial olivine-pyroxene texture (OZ1), scale: 100 μm; e) granular-platy texture, scale: 100 μm; f) granular-fibrous texture (OZ5), scale: 100 μm.

between the two chondrite types: in Knyahinya objects, they reach a maximum of 1.1 wt%, but are as high as 4.7 wt% in Ouzina objects.

Devitrified Glass

Glass in Knyahinya objects show a turbid aspect and contain between 61 and 67 wt% SiO_2, 15–23 wt% Al_2O_3, 6–9 wt% Na_2O, and 2–4.7 wt% CaO. Object OZ8 is the only one in Ouzina with glass; it is a very Si-rich (88.8 wt%) mesostasis glass associated with crystals of plagioclase.

Plagioclase

Plagioclase occurring in Knyahinya and Ouzina objects is albite-oligoclase with $Ab_{81–88}$ and $Ab_{75–89}$, respectively.

Table 2. Representative EMP analyses of olivine, low-Ca and high-Ca pyroxene, glass, and plagioclase in wt%.

KNYAHINYA-olivine										
Object	KN1	KN1 (rim)	KN2	KN2 (rim)	KN3	KN6	KN7	KN12	KN15	KN17
SiO_2	39.2	38.4	38.6	38.4	38.4	39.1	38.8	38.4	38.5	36.4
TiO_2	b.d.	b.d.	0.03	0.03	0.05	b.d.	0.03	0.04	0.04	b.d.
Al_2O_3	b.d.	b.d.	b.d.	0.10	b.d.	0.28	b.d.	b.d.	b.d.	b.d.
Cr_2O_3	b.d	b.d.	b.d.	0.49	0.09	b.d.	b.d.	b.d.	b.d.	b.d.
FeO	21.8	22.2	22.1	22.3	22.3	22.6	22.8	22.2	22.8	23.3
MnO	0.46	0.48	0.48	0.48	0.44	0.49	0.46	0.46	0.48	b.d.
MgO	39.3	39.5	38.4	38.1	39.2	37.8	37.5	38.1	38.5	35.7
TOTAL	100.7	100.6	99.5	99.9	100.5	100.3	99.5	99.1	100.2	95.3
XFA	0.24	0.24	0.24	0.25	0.24	0.25	0.25	0.25	0.25	0.27
XFO	0.76	0.76	0.76	0.75	0.76	0.75	0.75	0.75	0.75	0.73

OUZINA-olivine						
Object	OZ1	OZ2	OZ4	OZ5	OZ6	OZ8
SiO_2	36.2	36.3	36.1	36.5	36.1	36.2
TiO_2	0.08	0.02	0.03	0.03	b.d.	0.06
Al_2O_3	b.d.	b.d.	b.d.	0.26	b.d.	b.d.
Cr_2O_3	0.07	0.08	0.05	0.05	0.1	0.03
FeO	33.8	33.7	33.5	33.4	33.6	33.7
MnO	0.40	0.42	0.42	0.42	0.4	0.43
MgO	28.5	28.8	28.6	27.9	29.2	29.0
NiO	0.22	0.23	0.24	0.17	0.2	0.20
TOTAL	99.27	99.58	98.96	98.8	99.7	99.6
XFA	0.40	0.40	0.40	0.40	0.39	0.39
XFO	0.60	0.60	0.60	0.60	0.61	0.61

KNYAHINYA low-Ca pyroxene												
Object	KN1	KN2	KN6	KN7	KN8	KN9	KN12	KN13	KN15	KN16	KN17	KN21
SiO_2	56.1	55.9	56.3	56.1	56.4	56.3	56.0	54.4	55.8	56.0	55.0	56.5
TiO_2	0.1	0.11	0.1	0.17	0.12	0.1	0.12	0.26	0.15	0.13	0.11	0.11
Al_2O_3	0.1	0.13	0.1	0.16	0.17	0.2	0.10	0.39	0.12	0.13	0.35	0.12
Cr_2O_3	0.1	0.06	0.1	0.11	0.08	0.2	0.03	1.05	0.16	0.10	0.11	0.11
FeO	13.9	14.0	14.2	14.1	14.3	12.6	13.5	14.1	14.2	13.9	13.3	14.1
MnO	0.5	0.51	0.5	0.50	0.46	0.5	0.52	0.47	0.51	0.49	0.49	0.52
MgO	28.5	27.7	28.0	28.3	27.1	28.0	28.7	27.8	27.9	28.7	28.8	27.6
CaO	0.6	0.81	0.7	0.58	0.56	3.5	0.68	0.87	0.64	0.77	1.22	0.68
Na_2O	b.d.	0.03	b.d.	b.d.	0.03	0.1	b.d.	0.10	b.d.	0.05	0.08	b.d.
K_2O	100.0	99.3	99.9	100.0	99.3	101.4	99.7	99.5	99.56	100.2	99.5	99.7
TOTAL												
WO	1.15	1.60	1.35	1.13	1.12	6.66	1.32	1.71	1.26	1.49	2.34	1.35
EN	77.00	76.06	76.29	76.71	75.72	74.01	77.41	75.94	76.19	76.89	76.97	76.11
FS	21.86	22.35	22.36	22.16	23.16	19.33	21.27	22.35	22.56	21.62	20.69	22.55
JD	0.07	0.21	0.07	0.07	0.22	0.00	0.14	0.00	0.00	0.35	0.00	0.07

KNYAHINYA high-Ca pyroxene						
Object	KN2	KN6	KN8	KN9	KN15	KN21
SiO_2	52.6	53.4	55.2	57.2	53.1	54.5
TiO_2	0.5	0.6	0.2	0.5	0.8	0.5
Al_2O_3	0.8	0.8	0.9	1.1	0.9	0.9
Cr_2O_3	0.8	1.0	0.5	0.9	0.9	0.6
FeO	5.9	5.9	4.1	4.8	5.3	5.4
MnO	0.4	0.3	0.2	0.7	0.7	0.1
MgO	17.3	16.1	15.5	12.3	14.7	14.5
CaO	20.6	20.6	22.8	21.7	22.0	22.2
Na_2O	0.1	0.1	0.2	b.d.	0.2	0.4
K_2O	0.3	0.3	0.2	0.3	0.6	0.5
TOTAL	99.4	99.2	99.8	99.6	99.1	99.6

Table 2. *Continued*. Representative EMP analyses of olivine, low-Ca and high-Ca pyroxene, glass, and plagioclase in wt%.

KNYAHINYA high-Ca pyroxene						
Object	KN2	KN6	KN8	KN9	KN15	KN21
WO	41.48	43.08	47.71	50.33	46.68	47.57
EN	48.53	46.72	45.23	39.77	43.46	43.25
FS	9.99	10.20	7.06	9.90	9.86	9.18
JD	0.00	1.05	1.20	0.00	1.21	2.64
OUZINA high-Ca pyroxene						
Object	OZ1	OZ2	OZ4	OZ5	OZ6	OZ8
SiO_2	51.8	54.2	53.8	53.7	52.5	55.0
TiO_2	0.44	0.05	0.11	0.5	0.13	0.5
Al_2O_3	3.0	0.35	0.38	3.7	0.75	4.7
Cr_2O_3	0.42	0.69	0.46	1.0	0.58	0.2
FeO	7.8	6.8	7.2	6.3	7.9	6.3
MnO	0.16	0.15	0.17	0.1	0.14	0.2
MgO	14.2	15.7	15.0	13.6	16.2	12.9
CaO	22.1	22.6	22.1	20.6	21.7	19.0
Na_2O	0.70	0.55	0.47	1.2	0.58	1.5
K_2O	b.d.	b.d.	b.d.	0.1	b.d.	0.1
TOTAL	100.7	101.1	99.7	100.8	100.4	100.4
WO	45.98	45.22	45.39	46.34	43.01	45.18
EN	41.13	43.84	42.81	42.43	44.62	42.76
FS	12.89	10.94	11.80	11.23	12.37	12.06
JD	5.00	0.00	3.37	9.16	0.00	11.60

KNYAHINYA-devitrifed glass							OUZINA-glass
Object	KN3	KN7	KN8	KN16	KN17	KN21	OZ8
SiO_2	61.3	65.1	66.8	63.6	66.0	66.5	88.8
TiO_2	0.4	0.1	0.06	b.d.	0.06	0.1	b.d.
Al_2O_3	20.4	19.8	20.7	15.0	19.6	18.7	b.d.
Cr_2O_3	0.5	b.d.	0.06	0.2	0.06	0.2	b.d.
FeO	2.3	1.0	1.07	4.3	1.01	2.3	0.71
MnO	0.1	b.d.	b.d.	0.1	0.03	b.d.	0.04
MgO	1.4	1.8	1.61	8.2	1.53	4.4	0.20
CaO	2.9	3.5	4.0	1.8	4.7	2.7	0.57
Na_2O	9.2	8.2	5.9	7.5	6.1	5.4	b.d.
K_2O	0.5	0.8	0.84	0.2	0.45	0.7	b.d.
TOTAL	99.0	100.3	101.0	100.8	99.6	101.0	90.3

KNYAH1NYA-plagioclase				
Sample	KN1	KN2	KN6	KN13
SiO_2	66.9	66.2	64.7	64.1
TiO_2	b.d.	0.03	b.d.	0.1
Al_2O_3	22.8	20.9	20.7	19.2
FeO	0.8	0.72	1.8	1.7
MnO	b.d.	0.03	0.1	0.1
MgO	0.5	0.12	2.5	2.2
CaO	2.1	1.98	2.3	2.8
Na_2O	6.7	10.1	8.2	9.6
K_2O	0.6	0.46	0.9	0.4
TOTAL	100.4	100.5	101.1	100.0
AB	81.30	87.80	81.80	84.30
AN	13.80	9.50	12.50	13.70
OR	4.90	2.60	5.70	2.10

Table 2. *Continued*. Representative EMP analyses of olivine, low-Ca and high-Ca pyroxene, glass, and plagioclase in wt%.

OUZINA-plagioclase						
Sample	OZ1	OZ2	OZ4	OZ5	OZ6	OZ8
SiO_2	64.9	64.1	62.4	61.3	62.3	65.7
TiO_2	b.d.	0.06	0.02	0.11	b.d.	b.d.
Al_2O_3	22.5	19.8	21.0	18.8	21.7	21.8
FeO	1.08	1.34	0.76	2.6	1.27	0.96
MnO	0.02	0.03	b.d.	0.02	0.03	b.d.
MgO	0.04	1.33	0.14	2.8	0.09	0.02
CaO	3.0	4.3	1.66	4.9	3.4	2.5
Na_2O	9.7	9.0	12.6	8.2	10.2	9.7
K_2O	0.52	0.98	0.92	0.38	1.11	0.65
TOTAL	101.8	100.9	99.4	99.1	100.2	101.4
AB	82.80	75.00	89.20	73.50	79.60	84.10
AN	14.30	19.60	6.50	24.30	14.70	12.20
OR	2.90	5.40	4.30	2.20	5.70	3.70

Reference: b.d. = below detection limit.

Bulk Major and Minor Element Composition

Major element compositions of objects from Knyahinya are similar to the mean value of the nonporphyritic objects (Table 3) in UOCs (Engler et al. 2007). SiO_2 contents range from 41 to 59 wt%, Al_2O_3 contents from 2 to 4 wt%, FeO contents from 11 to 20 wt%, MgO contents from 19 to 34.5 wt%, and CaO contents from 1 to 7.6 wt%. The objects from Ouzina have higher FeO contents than the Knyahinya objects, up to 38 wt%, and lower MgO contents, from 12 to 19 wt% (Table 3, Fig. 2a). CaO contents range from 1.6 to 11 wt%. In two objects, OZ8 and OZ5, Al_2O_3 contents are anomalously high, reaching 7 to 9 wt%. The mean values for CaO and Al_2O_3 in all Ouzina objects are clearly higher than in the objects of Knyahinya (Fig. 2a), with CaO + Al_2O_3 contents showing some variation depending on the glass/feldspar ratio of the objects. In Knyahinya, 4 of 13 analyzed objects contain $Na_2O > 1$ wt% (KN1, KN2, KN3, KN7). In Ouzina objects, the Na_2O content is highly variable and reaches a maximum of 3.9 wt% (Fig. 2b).

Bulk Lithophile Trace Element Composition

Normalized abundances of objects having similar trace element patterns are plotted together in the same diagram.

Knyahinya Objects

Objects KN1, KN6, KN8, KN9, KN13, and KN16 (Table 4, Fig. 3a) have strongly fractionated refractory lithophile trace element abundance patterns with strong negative Y anomalies, and positive U, Ta, and Nb anomalies. LREE show variable but smooth fractionations relative to CI chondrites in most objects: In KN1 and KN13 abundances decrease smoothly from La to Sm, whereas in KN9, KN8, and KN16 they show a smooth increase, and no fractionation in KN6. A positive Eu anomaly is present in all samples, but this anomaly is larger in objects KN1 and KN13 compared with the others. The more refractory of the volatile elements (Sr, Ba) as well as the moderately volatile elements (Mn, V, and Cr) are unfractionated from CI abundances except for Cr abundances in KN9 and KN6, which are depleted relative to moderately volatile elements. In most objects, the elements Rb and Cs are depleted relative to other moderately volatile elements.

The objects KN2, KN7, KN12, KN16, KN17, and KN21 are plotted together in Table 4 and Fig. 3b. Two analyses were made of KN17, one of the barred olivine portion of the object (KN17-BO), and another of the barred pyroxene portion of the object (KN17BPx). The trace element patterns of these objects are somewhat similar to those described above. All show a pronounced negative Y anomaly and a positive U anomaly, but do not have positive Th and Nb anomalies. The more refractory as well as the moderately volatile elements, Sr, Ba, Mn, and V are nearly unfractionated with respect to CI concentrations, and abundances decrease with increasing volatility for Cr, Rb, and Cs (except for KN2, which has a negative Cr anomaly).

The barred olivine objects KN15 and KN3 (Table 4, Fig. 3c) have distinctive trace element abundance patterns that differ from the other Knyahinya objects. For KN15, in addition to the bulk analyses, glass was also analyzed (Fig. 3c). The glass shows an enrichment of Sc and Ca relative to the other elements, but lacks the

Table 3. Bulk major element composition of individual objects in equilibrated ordinary and Rumuruti chondrites.

	Knyahinya												
Chondrite object	KN1	KN2	KN3	KN6	KN7	KN8	KN9	KN12	KN13	KN15	KN16	KN17	KN21
SiO_2	52.4	41.0	46.7	50.4	51.5	59.1	56.8	56.0	52.2	49.6	57.5	55.1	56.6
TiO_2	0.13	0.03	0.08	0.3	0.1	0.3	0.3	0.3	0.3	0.4	0.1	0.2	0.3
Al_2O_3	2.7	1.88	2.30	2.4	2.4	2.7	2.4	2.7	2.1	4.0	2.1	2.2	2.6
Cr_2O_3	0.25	0.06	1.72	0.4	0.2	0.2	0.5	0.6	0.7	0.5	0.4	0.6	0.7
FeO	14.2	20.3	17.2	16.3	16.5	11.6	11.0	13.7	18.0	15.4	13.9	14.4	15.1
MnO	0.40	0.45	0.43	0.4	0.4	0.5	0.4	0.4	0.6	0.5	0.3	0.2	0.3
MgO	25.4	34.5	29.9	21.7	23.3	19.2	19.3	21.7	22.0	22.6	20.4	21.2	20.4
CaO	2.6	1.11	1.84	7.1	2.6	5.5	7.6	3.5	1.2	4.6	3.9	4.6	2.6
Na_2O	1.23	1.19	1.21	0.3	1.5	0.1	0.8	0.3	0.5	0.6	0.4	0.2	b.d.
K_2O	0.07	0.03	0.05	0.2	0.1	0.1	0.2	0.2	0.1	0.3	0.2	0.3	0.3
P_2O_5	0.03	0.09	0.06	0.3	0.1	0.2	0.2	0.1	0.0	0.4	0.1	0.1	0.2
Nl	0.24	0.03	0.08	0.1	0.2	0.2	0.2	0.2	0.5	0.3	0.1	0.4	0.2
Total	99.6	100.6	101.6	99.9	98.9	99.7	99.7	99.7	98.2	99.2	99.4	99.5	99.3

	Ouzina						
Chondrite	OZ1	OZ2	OZ4	OZ5	OZ6	OZ8	OZ9
SiO_2	41.3	43.9	51.3	48.8	39.5	41.3	38.1
TiO_2	0.3	0.2	0.4	0.4	0.3	0.4	0.2
Al_2O_3	3.9	1.6	4.5	8.7	1.4	7.4	1.1
Cr_2O_3	0.4	0.6	0.5	0.8	0.5	0.7	0.4
FeO	31.4	28.8	16.7	13.1	32.2	24.7	38.3
MnO	0.5	0.5	0.5	0.4	0.3	0.6	0.4
MgO	18.6	18.4	13.1	11.9	19.4	15.7	17.4
CaO	1.6	5.0	11.0	10.9	4.5	3.7	2.8
Na_2O	0.8	0.1	0.8	3.9	0.2	3.7	0.2
K_2O	0.2	0.1	0.5	0.5	0.2	0.4	0.2
P_2O_5	0.2	b.d.	0.2	0.2	0.4	0.3	0.2
Nl	0.1	0.4	0.2	0.2	0.2	0.6	0.4
Total	99.3	99.6	99.7	99.8	99.1	99.5	99.6

Reference: b.d. = below detection limit.

positive U anomaly that is present in the bulk object. In the bulk object the negative Y anomaly is also present, which seems to be characteristic of Knyahinya objects. The moderately volatile elements show a tendency for decreasing abundances with increasing volatility.

The barred olivine chondrule KN3 is exceptional because it contains a large apatite crystal. The trace element contents of the barred olivine and the enclosed apatite crystal in KN3 (Fig. 3d) show complementary patterns, that are strongly fractionated. The apatite crystal hosts Y as well as REE, except for Eu. The barred olivine portion of the chondrule hosts the more refractory lithophile elements and most of the moderately volatile elements.

Ouzina Objects

Refractory lithophile trace element (including REE) abundances of all objects in Ouzina (except for OZ8, the barred olivine object) vary between 0.7 and 10× CI and show a very similar fractionation pattern (Table 4, Fig. 4a). The LREE are usually depleted relative to the more refractory elements, but to a lesser extent than in the objects from Knyahinya. The HREE show a smooth continuous increase from Gd to Lu, with generally only a slight or no Eu anomaly (slight negative Eu anomalies occur in objects OZ4, OZ5, and OZ6). Y and Th anomalies are the most common. The moderately volatile elements are fractionated with a slight trend to a volatility-dependent depletion. Strontium and Ba commonly have the same abundance levels compared with the other elements. Mn is depleted relative to other moderately volatile elements in the majority of objects and Rb is enriched only in OZ8, OZ2, OZ4, and OZ5.

The normalized elemental contents of the barred olivine object OZ8 are plotted with the coexisting glass in Fig. 4b. The elemental abundances of the barred olivine object are about 4–5× CI and those of the glass about 10× CI. Refractory lithophile trace elements including the REE have relatively flat patterns. The moderately volatile elements Mn, V, Cr, Rb Cs, and W are depleted relative to the refractory elements in the olivine and glass, but with positive V and Rb anomalies.

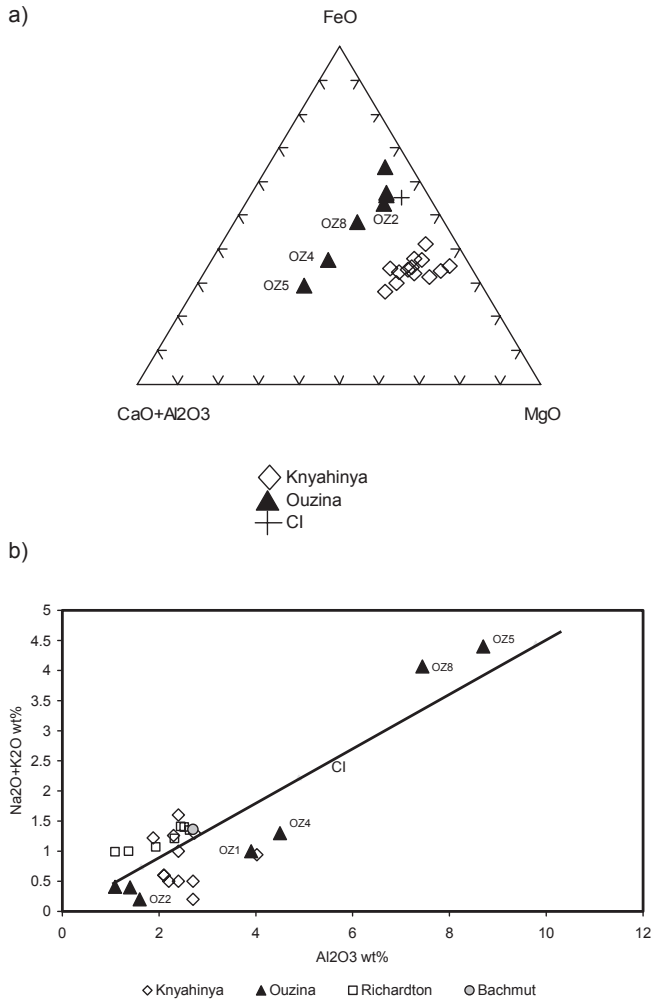

Fig. 2. a) Bulk compositions of Knyahinya and Ouzina objects projected onto the ($CaO + Al_2O_3$) – MgO – FeO planes. In addition, the bulk content of Orgueil is plotted as a primitive reference material (Anders and Grevesse 1989). b) Bulk contents of alkalis ($Na_2O + K_2O$) versus Al_2O_3 compared with the corresponding Cl abundance ratio (Anders and Grevesse 1989). The bulk contents of nonporphyritic chondrules of Richardton (Evensen et al. 1979) and Bachmut (Kurat et al. 1987) are shown for comparison.

DISCUSSION

Rumuruti (R) chondrites have mineralogical, geochemical, and isotopic characteristics that distinguish them from carbonaceous, ordinary, and enstatite chondrites (e.g., Rubin and Kallemeyn 1989; Bischoff et al. 1994, 2006, 2011; Schulze et al. 1994; Kallemeyn et al. 1996). In particular, they are more oxidized than perhaps any other chondrite group (e.g., Schulze et al. 1994). Evidence for the high state of oxidation includes negligible amounts of metallic Fe-Ni, a high abundance of NiO-bearing olivine, and the presence of abundant hornblende and minor biotite (e.g., Mikouchi et al. 2007; McCanta et al. 2008). The whole rock $\Delta^{17}O$ value is the highest of any chondrite group (Schulze et al. 1994; Greenwood et al. 2000).

Most R chondrites (except Carlisle Lake, Weisberg et al. 1991) are brecciated and contain equilibrated R5 and R6 clasts (Kallemeyn et al. 1996; Bischoff et al. 2006, 2011). Many are regolith breccias showing light/dark structure and solar wind implanted rare gasses (Weber and Schultz 1995). They are characterized by moderate abundances of volatile elements, a low chondrule/matrix modal abundance ratio, rather small chondrules (approximately 400 μm in apparent diameter), and scarce refractory inclusions (e.g., Rubin and Kallemeyn 1989; Weisberg et al. 1991; Bischoff et al. 1994, 2011; Schulze et al. 1994; Greenwood et al. 1996; Kallemeyn et al. 1996).

R chondrites share several geochemical features (e.g., contents of moderately volatile elements Na and Mn) with ordinary chondrites (OCs) (Bischoff et al. 2011), but some of their chemical characteristics do not follow the H-L-LL sequence (Rubin and Kallemeyn 1989). Also, the high abundance of matrix material and contents of Zn and Se in R chondrites resemble that of carbonaceous chondrites (CCs) more closely than OCs (e.g., Bischoff et al. 1994). On the other hand, the oxygen isotopic composition of chondrules in R chondrites and OCs show a stronger relationship than that between R chondrites and CCs (Isa et al. 2011). Nonetheless, small but significant differences in oxygen isotopes between R and OCs exclude formation of R chondrites from OCs simply by oxidation (e.g., Schulze et al. 1994).

The existing data therefore suggest that R chondrites are formed in an environment similar to, but somewhat different than, OCs. Here, we explore the differences between R chondrites and OCs further, by examining the chemical data for nonporphyritic chondrules and related objects in Ouzina and Knyahinya.

Most chondrules in equilibrated chondrites have been modified by secondary processes such as interactions between the chondrule and nebular gas (e.g., replacement of olivine by pyroxene and vice versa) and aqueous alteration or thermal metamorphism on their parent bodies (e.g., Kurat 1969; McSween and Labodka 1993; Huss et al. 2006). These processes tend to obliterate primary mineralogical features through, for example, the activation of exchange reactions. These reactions are present in equilibrated chondrites but they can be best identified or expected to be preserved only where the reactions remained incomplete, as in the case of the least altered, unequilibrated ordinary chondrites. In equilibrated chondrites, an examination of secondary processing must rely more on geochemical data.

In the following paragraphs we explore the question: Do the nonporphyritic objects in the equilibrated Knyahinya and Ouzina chondrites preserve geochemical

Table 4. Trace element analyses of objects and phases in Knyahinya and Ouzina chondrites (LA-ICP-MS analyses in ppm-except Ca and Ti in wt%).

Chondrite	Knyahinya																	
object	KN1	KN2c	KN2r	KN3	KN3ol	KN6	KN7	KN8	KN9	KN12	KN13	KN3ap	KN15	KN15gl	KN16	KN17BPx	KN17BO	KN21
Zr	7.07	10.59	0.80	6.88	0.80	19.13	8.27	13.62	15.69	9.57	6.38	0.01	8.28	18.68	9.25	11.78	3.72	6.86
Hf	0.17	0.32	0.02	0.23	0.06	0.58	0.22	0.25	0.34	0.21	0.16		0.24	0.57	0.24	0.29	0.09	0.18
Sc	5.93	20.99	3.73	3.02		30.93	14.07	19.52	23.59	17.20	6.63		16.12	47.79	17.79	26.22	7.80	12.02
Ca	0.61	3.02	0.12	0.65		4.68	2.09	4.06	4.72	2.60	0.53	1.91	2.63	6.86	2.86	5.33	0.99	1.73
Y	0.42	1.83	0.09	0.05		2.07	1.03	1.62	1.78	1.16	0.31	15.40	1.26	3.07	1.11	1.83	0.42	0.69
Th	0.09	0.04	b.d	0.01		0.08	0.12	0.09	0.18	0.10	0.10	0.05	0.05	0.06	0.12	0.12	0.04	0.07
U	0.04	0.02	0.01	0.03	0.02	0.04	0.04	0.07	0.08	0.08	0.04	0.01	0.04	0.01	0.03	0.07	0.02	0.06
Ti	0.07	0.05	0.01	0.30	0.03	0.09	0.11	0.09	0.09	0.09	0.11	0.00	0.07	0.11	0.11	0.12	0.08	0.08
Ta	0.08	0.04	b.d	0.14	0.02	0.12	0.03	0.04	0.05	0.04	0.04	0.00	0.04	0.05	0.03	0.03	0.02	0.02
Nb	1.43	0.69	0.20	3.54		2.73	0.56	0.99	1.14	0.87	1.01	0.00	0.67	0.86	0.51	0.56	0.41	0.51
La	0.08	0.25	0.01	0.03		0.25	0.10	0.11	0.12	0.09	0.04	3.16	0.16	0.33	0.06	0.12	0.04	0.04
Ce	0.17	0.63	0.04	0.07		0.69	0.28	0.37	0.40	0.34	0.09	8.52	0.54	1.02	0.22	0.42	0.14	0.16
Pr	0.02	0.09	b.d	0.01		0.10	0.04	0.06	0.06	0.05	0.01	1.22	0.07	0.17	0.04	0.07	0.02	0.03
Nd	0.10	0.49	b.d	0.02		0.51	0.23	0.34	0.35	0.24	b.d	5.88	0.36	0.97	0.20	0.39	0.08	0.12
Sm	0.02	0.19	b.d	0.01		0.18	0.08	0.12	0.15	0.09	0.02	1.81	0.14	0.39	0.08	0.14	b.d	0.06
Eu	0.06	0.09	0.01	0.19		0.11	0.07	0.08	0.07	0.06	0.07	0.09	0.09	0.15	0.06	0.07	0.04	0.06
Tb	0.01	0.04	b.d	0.00		0.05	0.02	0.04	0.04	0.02	0.01	0.40	0.03	0.07	0.03	0.04	0.01	0.01
Gd	0.04	0.25	b.d	b.d		0.27	0.13	0.19	0.22	0.12	0.02	2.47	0.17	0.42	0.13	0.22	0.05	0.08
Dy	0.08	0.31	0.03	0.01		0.38	0.18	0.31	0.32	0.18	0.04	2.84	0.22	0.46	0.20	0.33	0.07	0.12
Ho	0.02	0.07	b.d	0.00		0.08	0.04	0.06	0.08	0.04	0.01	0.59	0.05	0.11	0.04	0.08	0.02	0.03
Er	0.06	0.21	b.d	b.d		0.26	0.14	0.21	0.23	0.15	0.05	1.69	0.15	0.43	0.14	0.22	0.06	0.09
Tm	0.01	0.03	0.00	0.00		0.04	0.02	0.03	0.04	0.03	0.01	0.23	0.03	0.06	0.02	0.04	0.01	0.02
Yb	0.10	0.24		0.01		0.35	0.18	0.30	0.32	0.23	0.11	1.38	0.19	0.47	0.20	0.32	0.10	0.15
Lu	0.02	0.04	0.01	0.00		0.06	0.03	0.04	0.05	0.04	0.02	0.18	0.03	0.06	0.03	0.05	0.02	0.03
Sr	9.0	13.7	1.5	31.0	1.8	15.0	9.5	10.8	9.9	9.4	11.1	1.7	13.6	25.9	9.4	11.8	5.6	8.8
Ba	3.2	4.4	0.5	10.0	1.1	5.0	3.4	3.5	3.1	3.3	4.1	0.0	4.8	7.8	3.1	3.8	2.1	3.4
Mn	0.31	0.24	0.39	0.24	0.34	0.26	0.28	0.29	0.27	0.33	0.32	0.00	0.34	0.25	0.30	0.29	0.38	0.34
V	32.9	62.6	6.96	196	22.9	101	85.2	76.6	85.7	86.1	82.6	0.25	83.6	146	90.1	106	68.1	80.7
Cr	1180	853	304	17303	1404	1140	2760	1380	1500	3100	4192	12.2	2252	2086	3639	3565	3618	3367
Rb	1.44	2.15	0.52	4.38		2.53	1.55	1.65	1.50	1.90	2.11	0.03	2.85	3.78	1.93	2.44	1.19	2.01
Cs	b.d	0.02	b.d	0.04		0.02	b.d	0.02	b.d	0.06	b.d	b.d	0.04	b.d	b.d	b.d	0.02	0.03
W	b.d	0.05	0.07	0.03		0.04	0.01	0.01	b.d	0.06	b.d	0.00	0.04	0.07	b.d	0.02	0.03	0.02

Chondrite	Ouzina							
object	OZ1	OZ2	OZ2ol	OZ4	OZ5	OZ6	OZ8	OZ8gl	OZ8ol
Zr	9.47	8.48	3.34	12.23	36.89	13.32	18.33	43.90	1.67
Hf	0.38	0.23	0.14	0.31	0.86	0.36	0.52	1.16	0.08
Sc	19.90	21.60	10.26	28.14	46.49	29.60	20.13	40.54	b.d
Ca	0.00	0.01	0.00	0.01	0.01	0.00	0.00	0.01	0.00
Y	2.60	4.39	1.10	7.72	9.12	4.26	5.41	13.92	0.49
Th	0.05	0.06	b.d	0.08	0.30	0.10	0.14	0.28	0.02

Table 4. *Continued*. Trace element analyses of objects and phases in Knyahinya and Ouzina chondrites (LA-ICP-MS analyses in ppm-except Ca and Ti in wt%).

Chondrite	Ouzina								
object	OZ1	OZ2	OZ2ol	OZ4	OZ5	OZ6	OZ8	OZ8gl	OZ8ol
U	0.01	b.d	b.d	0.01	0.03	0.01	0.04	0.06	0.01
Ti	0.07	0.07	0.04	0.15	0.18	0.05	0.22	0.62	0.03
Ta	0.02	0.03	0.03	0.04	0.09	0.03	0.08	0.24	b.d
Nb	0.37	0.39	0.25	0.82	1.45	0.75	1.41	4.36	0.16
La	0.16	0.32	0.06	0.47	0.50	0.18	1.22	2.26	0.04
Ce	0.49	1.15	0.35	1.79	1.58	0.66	3.17	5.85	0.23
Pr	0.09	0.19	0.05	0.32	0.26	0.12	0.41	0.87	0.03
Nd	0.51	1.02	0.12	1.76	1.57	0.67	1.89	4.49	0.07
Sm	0.24	0.40	0.07	0.72	0.63	0.30	0.61	1.44	0.07
Eu	0.08	0.22	0.06	0.24	0.33	0.09	0.20	0.46	0.01
Tb	0.06	0.10	b.d	0.17	0.19	0.09	0.13	0.32	0.01
Gd	0.36	0.53	0.13	0.93	1.11	0.50	0.78	1.96	0.06
Dy	0.53	0.70	0.17	1.33	1.77	0.73	0.99	2.49	0.07
Ho	0.11	0.16	0.05	0.30	0.36	0.16	0.20	0.53	0.01
Er	0.29	0.53	0.16	0.89	1.15	0.52	0.58	1.42	b.d
Tm	0.05	0.08	0.02	0.13	0.16	0.08	0.08	0.21	b.d
Yb	0.33	0.58	0.17	0.95	1.13	0.49	0.58	1.49	0.07
Lu	0.05	0.08	0.03	0.11	0.16	0.08	0.08	0.19	0.02
Sr	12.8	15.7	2.0	17.3	34.8	10.9	40.0	72.6	6.1
Ba	3.7	5.6	0.4	5.0	8.2	1.8	7.5	15.9	1.4
Mn	0.19	0.13	0.23	0.15	0.10	0.17	0.12	0.06	0.22
V	75.8	98.5	59.7	118	132	68.1	79.6	166	17.5
Cr	3107	4235	3057	4657	3574	2079	1515	954	610
Rb	1.92	13.63	1.36	24.86	4.09	1.16	4.04	11.45	1.31
Cs	0.03	0.42	0.04	0.87	0.07	0.03	0.18	0.43	0.02
W	0.08	0.08	0.08	0.07	0.21	0.22	0.17	0.18	0.08

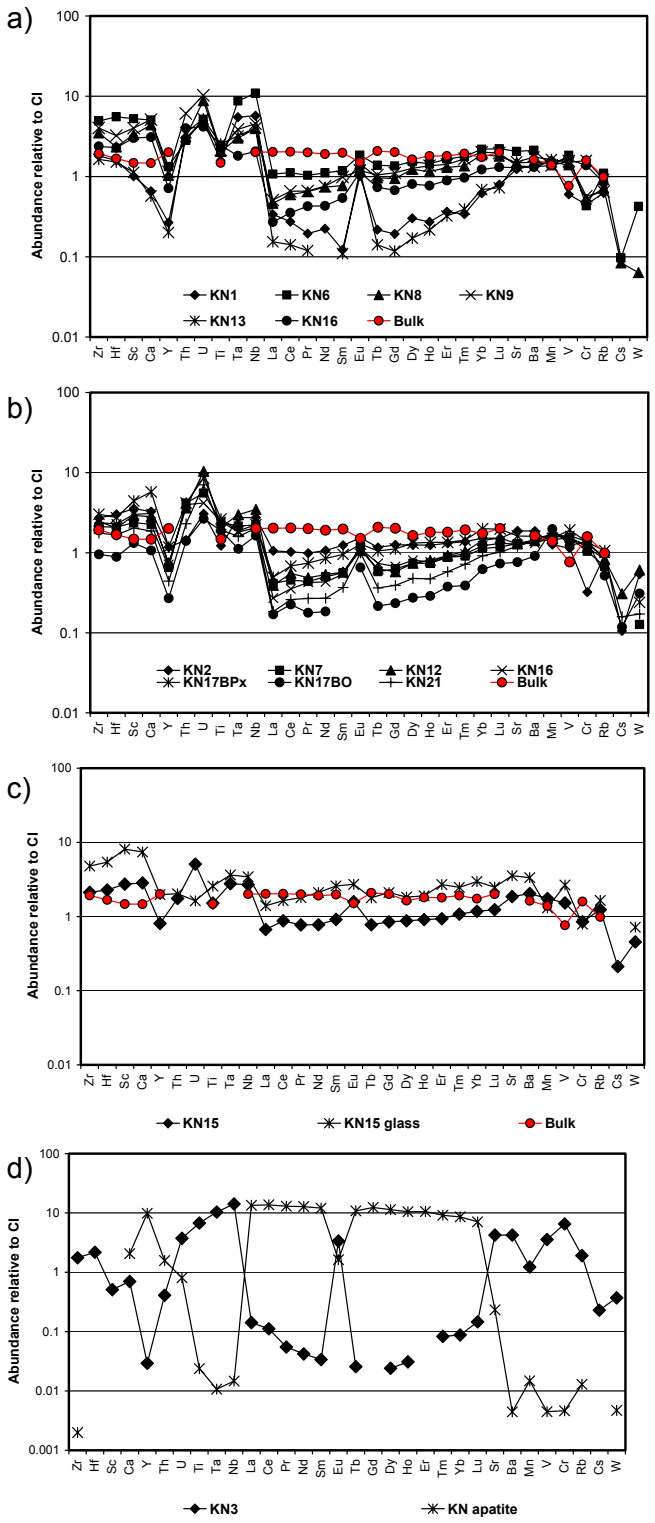

Fig. 3. Bulk (a–c) and glass-mineral (c–d) analyses of lithophile trace elements normalized to Cl abundances (here and in the following graphs normalizing data were taken from Lodders and Fegley 1998) in objects of the equilibrated Knyahinya chondrite. The bulk Knyahinya trace element abundance (Bulk) (Kallemeyn et al. 1989; Friedrich et al. 2003) is shown for comparison.

characteristics that reveal differences between the environments in which they were generated and/or processed?

Major Element Systematics

Major element trends on binary element plots for nonporphyritic chondrules and related objects from Knyahinya and Ouzina deviate from CI chondritic ratios (solar abundance ratio line) (Fig. 5). This is most probably due to disturbance of the primary compositions by secondary processes (e.g., Fe^{2+} exchange reactions or addition of alkalis) during re-equilibration of the chondrite.

The Knyahinya and Ouzina objects tend to be enriched in calcium relative to the CaO/Al_2O_3 CI chondritic ratio (Fig. 5a), which is preserved in most nonporphyritic objects from UOCs (Engler et al. 2007). As mentioned above, the mean values for CaO + Al_2O_3 in all Ouzina objects are higher than in the objects of Knyahinya (Fig. 2a). The variations of CaO and Al_2O_3 in the objects are probably a function of their glass/feldspar ratio, formed prior to secondary processing. All objects of Knyahinya are depleted in iron relative to CI chondritic ratio of FeO/Al_2O_3, similar to the primary ratios of some objects in UOCs (Fig. 5b). In contrast, the large scatter of FeO/Al_2O_3 in the Ouzina objects likely reflects secondary processing during which FeO was variably added at the expense of Mg during metasomatic reactions. Mg in the Knyahinya objects exhibits apparent equilibration with respect to the chondritic MgO/Al_2O_3, ratio, as objects KN1, KN6, KN7, KN16, and KN17 plot on or close to the solar abundance ratio line (Fig. 5c). However, their original composition was probably rich in MgO (as revealed by the MgO content of most nonporphyritic objects in UOCs) and, due to equilibration processes (Fe^{2+} exchange reactions), the MgO contents now plot close to the solar MgO/Al_2O_3 ratio. The objects of Ouzina show a large scatter far away from the cosmic MgO/Al_2O_3 abundance ratio line, consistent with Mg mobility during metasomatism (Fig. 5c).

Turning to the volatile elements, metasomatic addition of alkalis has created variable Na/K ratios in the objects. For a given chondrule, the final Na/K ratio depends on when and for how long it was exposed to an alkali-rich fluid or vapor. The sums of the volatile components K_2O + Na_2O do not show any correlation with refractory lithophile elements (e.g., Al_2O_3) in objects of the Knyahinya EOC (Fig. 2b). However, those of Ouzina scatter around the CI line. This correlation could indicate re-equilibration processes with a chondritic reservoir.

In summary, the differences in the chemical trends for the objects from Ouzina as compared with those in

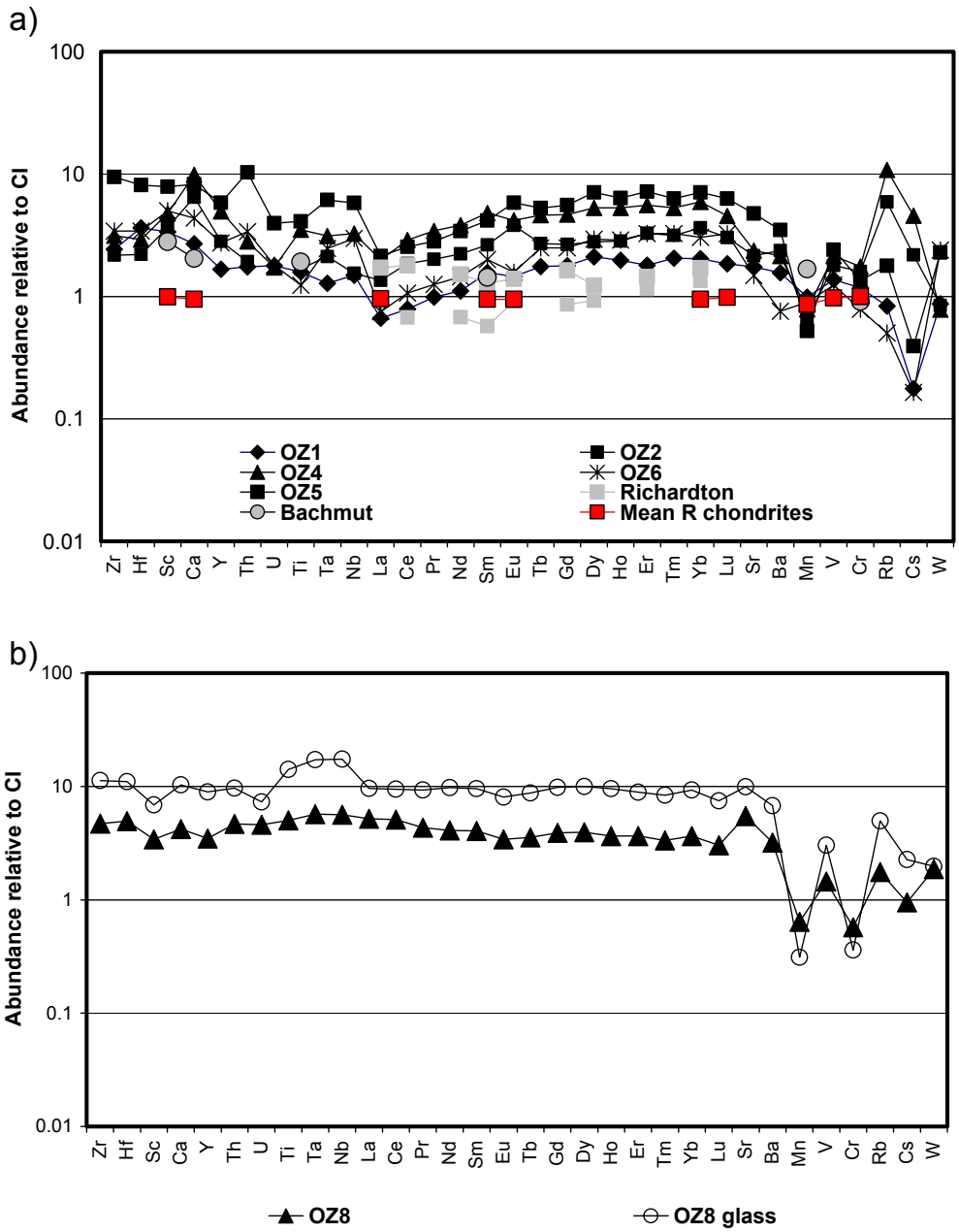

Fig. 4. Bulk (a–b) and glass (b) analyses of lithophile trace elements normalized to Cl abundances in objects of the equilibrated Ouzina chondrite. The mean trace element abundance of R chondrites (Mean R chondrites) (Kallemeyn et al. 1989), and the trace element abundances of bulk nonporphyritic objects of Bachmut (Kurat et al. 1987) and Richardton (Evensen et al. 1979) are also shown.

Knyahinya probably indicate that they were generated and/or processed in different environments.

Trace Element Systematics

Yb-Ce-Sc Ratios

The compatible/refractory element Yb is plotted against the incompatible/refractory element Ce in Fig. 6a, and against the compatible/refractory element Sc in Fig. 6b. Although Ce might appear to be a poor choice as representative of the LREE as compared with La (due to its redox-sensitive volatility), both incompatible elements exhibit similar trends (see inset in Fig. 6a). Our choice of Ce is based on the fact that La is highly mobile and also much less abundant than Ce.

The Knyahinya nonporphyritic chondrules have well-correlated Yb/Ce and Sc/Yb ratios that trend above the corresponding ratios for CI chondrites. The observed

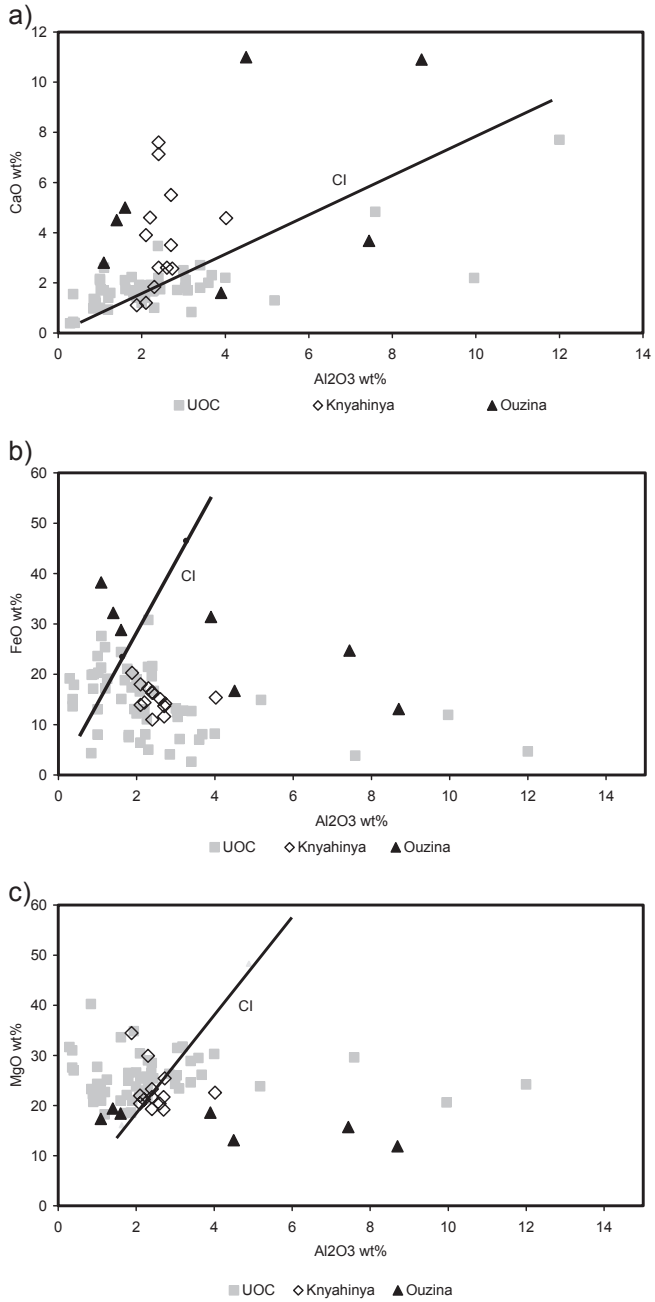

Fig. 5. Bulk a) CaO, b) FeO, and c) MgO versus Al_2O_3 ratios in the Knyahinya and Ouzina objects compared with CI chondrite abundances and the bulk contents of nonporphyritic objects of UOCs (Engler et al. 2007).

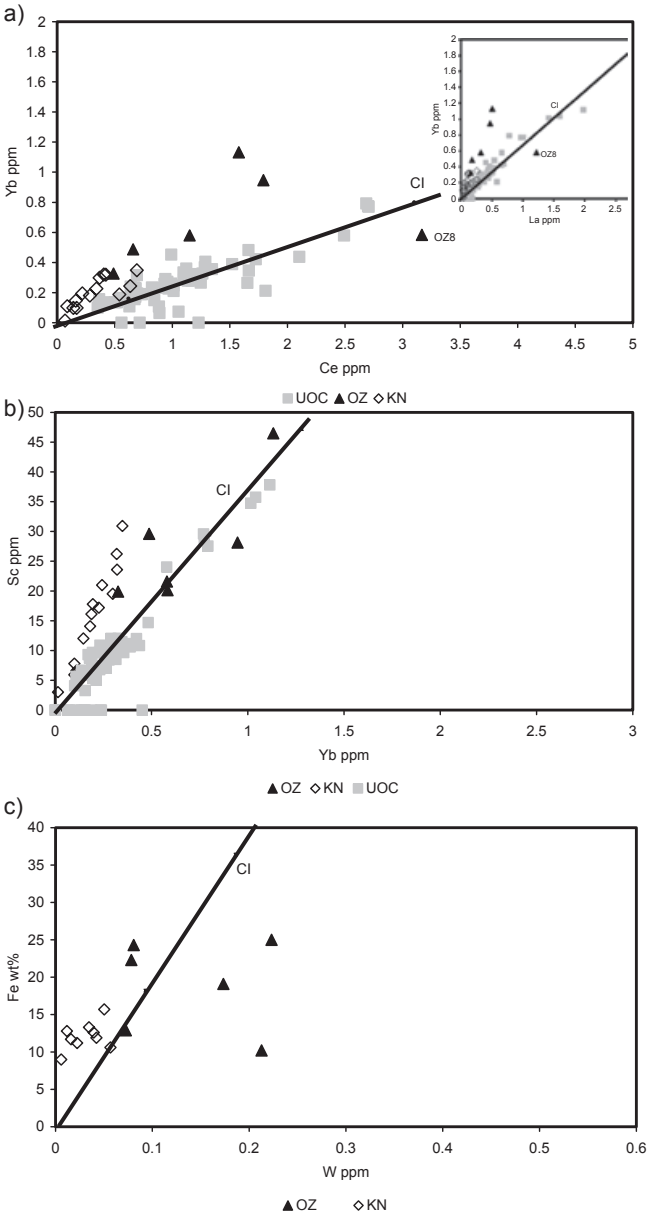

Fig. 6. Element correlation plots for a) Yb versus Ce (inset: Yb versus La); b) Sc versus Yb; c) Fe versus W. Data for nonporphyritic objects in unequilibrated ordinary chondrites (UOCs) (Engler et al. 2007) are shown for comparison.

steep Sc/Yb correlation could reflect the crystal-chemical preference of the pyroxene-dominated objects of Knyahinya for Sc relative to Yb. The correlation of Yb and Ce contents shows that the elements were slightly fractionated from the primordial ratio, similar to what has been observed in nonporphyritic objects in UOCs (Fig. 6a, Engler et al. 2007). Sc/Yb ratios for the Ouzina nonporphyritic chondrules scatter around the CI chondritic ratios (Fig. 6b) and show no correlation of Yb and Ce. Again, this indicates that the environments in which the objects of the Rumuruti chondrite evolved were different from those of the Knyahinya chondritic rocks.

Fe-W Ratios

A diagram of Fe versus W contents (Fig. 6c) provides some information concerning the redox conditions and history of W in the Knyahinya and

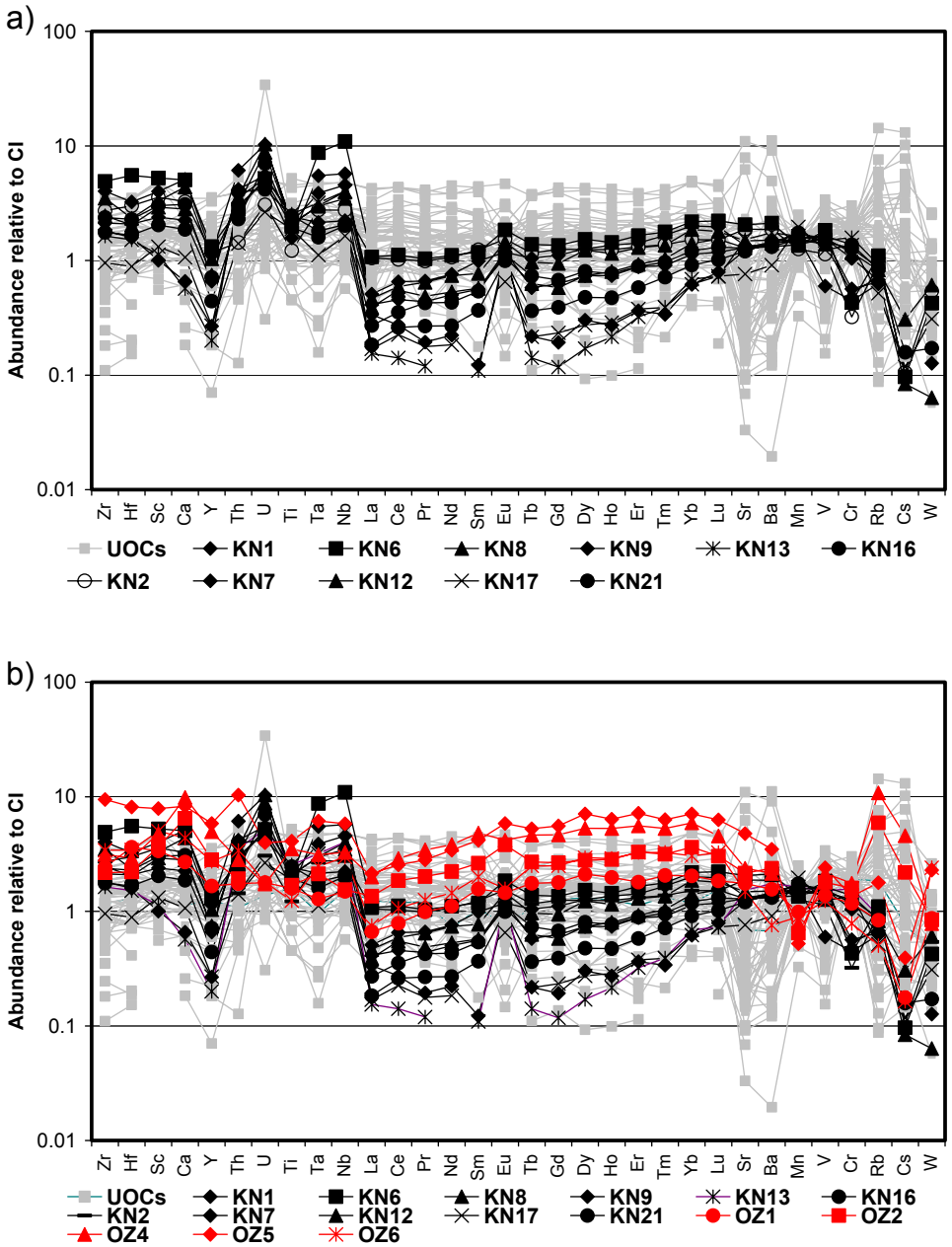

Fig. 7. Bulk analyses of lithophile trace elements normalized to Cl abundances of all studied objects in a) Knyahinya and b) Ouzina compared with those of UOCs (Engler et al. 2007).

Ouzina nonporphyritic chondrules. Fe/W ratios in the Knyahinya objects tend to be higher than the solar ratios, suggesting that Fe^{2+} was added to, or W removed from, the Knyahinya objects during sub-solidus metasomatic processes. The objects in Ouzina, in contrast, show more scatter with three chondrules exhibiting anomalously high W concentrations. Overall, despite their very low metal contents, Ouzina nonporphyritic chondrules are richer in W (0.9–2× CI) than those in Knyahinya (0.1–0.7× CI). The W enrichments can be explained by secondary processing under oxidizing conditions, where W becomes lithophile and is therefore incorporated preferentially into the silicate phases of the chondrules (e.g., Rambaldi et al. 1979).

LREE-HREE-HFSE Patterns

Individual nonporphyritic chondrules in Knyahinya and Ouzina have variable abundances of refractory, moderately volatile, and volatile lithophile elements, but the trace element abundance patterns of the different objects are relatively uniform within each chondrite (Fig. 7a). For Knyahinya, refractory element abundances

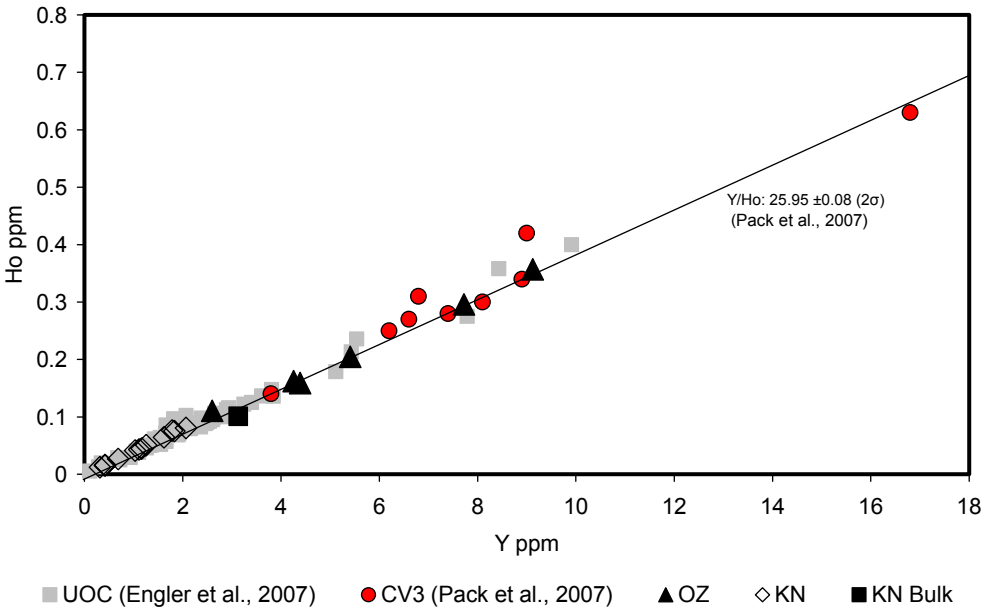

Fig. 8. Bulk Y versus Ho ratios of Knyahinya and Ouzina objects compared with CI (Y/Ho: 25.95 ± 0.08 (2σ), Pack et al. 2007). Bulk contents of nonporphyritic objects of UOCs (Engler et al. 2007) and CV3 Allende (Pack et al. 2007) are included.

vary considerably between 0.1 and 14× CI. But almost every object has a CI chondrite-normalized pattern that is depleted in LREE relative to the majority of the ultra-refractory elements, including Sc, Ca, and the high-field-strength elements (HFSEs; Zr, Hf, Th, U, Ti, Ta, Nb), as well as relative to the majority of HREE. All show variable positive Eu anomalies and a smooth continuous increase in enrichment of HREE from Gd to Lu. For Ouzina objects (Fig. 7b), ultra-refractory element abundances are similar to those in Knyahinya objects, but rare earth elements in Ouzina (approximately 0.8–8× CI) are more enriched than in Knyahinya (approximately 0.2–2× CI). Ouzina objects have CI chondrite-normalized REE patterns that are slightly LREE-depleted with small positive or negative Eu anomalies.

Compared with the bulk trace element abundance patterns of nonporphyritic chondrules from UOCs (Engler et al. 2007), those in Knyahinya and Ouzina indicate a more complicated genesis (Figs. 7a and 7b). The depletion trend of LREE with respect to HREE and HFSE documents variable degrees of LREE transport into an external mineral sink (e.g., Rambaldi et al. 1981) and restricted mobility of other refractory trace elements. The presence of "mysterite" and "holy smoke" (Laul et al. 1973; Higuchi et al. 1977; Rambaldi et al. 1981) in some chondrite matrices could indicate that this transport was a parent body process. The fact that Eu does not show large anomalies relative to the other REE in the Ouzina objects suggests that it was oxidized and thus behaved like the other +3 REE during secondary processing.

Moderately Volatile Elements

The moderately and highly volatile elements (Sr, Ba, Mn, V, Cr, Rb, Cs, W) show a volatility-dependent depletion in Knyahinya and Ouzina nonporphyritic chondrules, with normalized abundances tending to decrease from Sr to W (Figs. 7a and 7b). This pattern may reflect removal of the chondrules and related objects from the nebular gas before complete condensation of these elements. However, some of the objects exhibit fractionations that may reflect element mobility during metasomatic processes. In particular, the CI chondrite-normalized patterns for all of the Knyahinya objects show negative Cs anomalies, and some show negative Cr anomalies as well (Fig. 7a). All the Ouzina objects have negative Mn anomalies but near chondritic Cr and V normalized abundances, suggesting that these elements equilibrated with the chondritic reservoir during secondary processing. Some objects have negative Cs anomalies and others have positive Rb and Cs anomalies (Fig. 7b). The strongly fractionated Rb/Cs ratios (up to 10 x CI) in all studied objects (Fig. 7b) imply low original contents and restricted mobility of the large Cs ion. While Na_2O and K_2O were able to re-equilibrate with the chondritic system in Ouzina objects (Fig. 2b), the large Rb and Cs ions could not (Fig. 4a).

Tungsten abundances in all objects appear to be variable, similar to Rb and Cs. This is likely because W is an incompatible and volatile element under oxidizing conditions.

Y-Ho Ratios

Pack et al. (2007) showed that concentrations of Y and Ho are highly variable in porphyritic and nonporphyritic chondrules from unequilibrated ordinary and CV3 chondrites, whereas Y/Ho ratios (approximately 26) show very little variation. Because large fractionations of these two elements are not expected during thermal metamorphism (Blundy and Wood 2003), the Y and Ho concentrations in the nonporphyritic chondrules of Knyahinya and Ouzina most likely are a primary feature acquired during formation. Chondrules from Knyahinya have Y and Ho concentrations overlapping those of the majority of nonporphyritic chondrules in UOCs (Fig. 8). Chondrules from Ouzina have higher Y and Ho contents, more akin to those measured in the nonporphyritic chondrules of Allende CV3 chondrite (Pack et al. 2007). The Y/Ho ratios for all objects are approximately 26 (Knyahinya Y/Ho: 25.42 ± 1, 2σ, and Ouzina Y/Ho: 25.9 ± 1.4, 2σ) indicating that this ratio was similar in the nebular regions where nonporphyritic pyroxene, pyroxene/olivine microchondrules, and chondrule fragments from Knyahinya and Ouzina were formed.

CONCLUSIONS

All nonporphyritc chondrules of the equilibrated chondrites, L/LL5 Knyahinya and R4 Ouzina, have major and trace element abundances that are systematically fractionated relative to CI abundances largely as a result of late stage equilibration processes. This process, generally called "metamorphism," can be seen in the abundances of major and trace elements involving mobilization of incompatible elements. During secondary processing, incompatible trace elements—in particular the LREE—were removed from the chondrules to a trace element sink located outside the chondrules. This could have occurred before or after accretion. Whereas the LREE are mobile, the HREE and high-field-strength elements are less so and therefore remained fixed at their high primary abundances in the objects, producing the fractionated trace element patterns exhibited by many chondrules from Knyahinya and Ouzina.

Abundance pattern trends in the chondrules of the two chondrites are broadly similar but the small to absent Eu anomalies and the high abundance of W in Ouzina objects reflect processing under more oxidizing conditions.

The irregular abundance variations of the moderately volatile elements could reflect incomplete late stage metasomatic processes. These elements are mobile and thus are involved in vapor-solid exchange processes. FeO as well as the moderately volatile elements (e.g., V, Cr, Mn, as well as K, and Na) were probably added to the objects in differing amounts—depending on the redox conditions of the system—during metasomatic processes in equilibrium with a chondritic reservoir (e.g., Na + K).

All of the nonporphyritic chondrules from Knyahinya and Ouzina show undisturbed Y/Ho solar ratios, a feature that they share with the nonporphyritic chondrules of UOCs, attesting to the robustness of primary Y and Ho correlations during secondary processing.

Acknowledgments—We are grateful to A. Bischoff for constructive discussions. The manuscript benefited from the comments of M. Weisberg and A. Rubin. Financial support was received from FWF (P13975.GEO and P14938), Austria, CONICET (PIP 1645), Agencia (PICT212), CONICET-FWF International Cooperation Projects, Argentina, and the NSERC Discovery Grant Program (PJS). A. Engler received a visiting PhD research scholarship award from Memorial University.

Editorial Handling—Dr. A. J. Timothy Jull

REFERENCES

Anders E. and Grevesse N. 1989. Abundance of the elements: Meteoritic and solar. *Geochimica et Cosmochimica Acta* 53:197–214.

Berlin J., Jones R. H., Brearley A. J., and Spilde M. N. 2008. Determining bulk chemical compositions of chondrules by electron microprobe: Modal recombination versus defocused beam analyses. *Microscopy and Microanalysis* 14:110–111.

Bischoff A., Geiger T., Palme H., Spettel B., Schultz L., Scherer P., Loeken T., Bland P., Clayton R. N., Mayeda T. K., Herpers U., Meltzow B., Michel R., and Dittrich–Hannen B 1994. Acfer 217—A new member of the Rumuruti chondrite group (R). *Meteoritics* 29:264–274.

Bischoff A., Scott E. R. D., Metzler K., and Goodrich C. A. 2006. Nature and origins of meteoritic breccias. In *Meteorites and the early solar system II*, edited by Lauretta D. S. and McSween H. Y., Jr. Tucson, Arizona: The University of Arizona Press. pp. 679–712.

Bischoff A., Vogel N., and Roszjar J. 2011. The Rumuruti chodrite group. *Chemie der Erde* 71:101–133.

Blundy J. and Wood B. 2003. Partitioning of trace elements between crystals and melts. *Earth and Planetary Science Letters* 210:383–397.

Engler A., Kurat G., and Sylvester P. J. 2004. Trace element abundances in chondrules from Knyahinya (L/LL5) and Ouzina (R4). *Meteoritics & Planetary Science* 39:A37.

Engler A., Varela M. E., Kurat G., Ebel D., and Sylvester P. J. 2007. The origin of non-porphyritic pyroxene chondrules in UOCs: Liquid solar nebula condensates? *Icarus* 192:248–286.

Evensen N. M., Carter S. R., Hamilton P. J., O'Nions, R. K., and Ridley W. J. 1979. A combined chemical-petrological study of separates chondrules from the Richardton meteorite. *Earth and Planetary Science Letters* 42:223–236.

Friedrich J. M., Wang M. S., and Lipschutz M. E. 2003. Chemical studies of chondrites. V: Compositional patterns

for 49 trace elements in 14 L4-6 and 7 LL4-6 falls. *Geochimica et Cosmochimica Acta* 67:2467–2479.

Gooding J. L. and Keil K. 1981. Relative abundances of chondrule primary textural types in ordinary chondrites and their bearing on conditions of chondrule formation. *Meteoritics* 16:17–43.

Greenwood J. P., Rubin A. E., and Wasson J. T. 1996. The compositional classification of chondrites: VII. The R chondrite group. *Geochimica et Cosmochimica Acta* 60:2243–2256.

Greenwood J. P., Rubin A. E., and Wasson J. T. 2000. Oxygen isotopes in R-chondrite magnetite and olivine: Links between R chondrites and ordinary chondrites. *Geochimica et Cosmochimica Acta* 64:3897–3911.

Grossman J. N. 2000. Meteoritical Bulletin 84. *Meteoritics & Planetary Science* 35:A199.

Heyse J. V. 1978. The metamorphic history of LL-group ordinary chondrites. *Earth and Planetary Science Letters* 40:365–381.

Higuchi H., Ganapathy R., Morgan J. W., and Anders E 1977. "Mysterite": A late condensate from the solar nebula. *Geochimica et Cosmochimica Acta* 41:843–852.

Huss G. R., Rubin A. E., and Grossman J. N. 2006. Thermal metamorphism in chondrites. In *Meteorites and the early solar system II*, edited by Lauretta D. S. and McSween H. Y., Jr. Tucson, Arizona: The University of Arizona Press. pp. 567–586.

Isa J., Rubin A. E., Marin-Carbonne J., McKeegan K. D., and Wasson J. T. 2011. Oxygen isotopic compositions of R-chondrite chondrules (abstract #2623). 47th Lunar and Planetary Science Conference. CD-ROM.

Jackson S. 2001. The application of ND: YAG lasers in LA-ICP-MS. In *Laser ablation-ICPMS in the earth sciences, principles and application*, edited by Sylvester P. *Mineralogical Association of Canada*. Short course series. 29:29–45.

Jackson S., Longerich H. P., Dunning G. R., and Fryer B. J. 1992. The application of Laser-Ablation Microprobe-Inductively coupled plasma—Mass spectrometry (LAM-ICP-MS) to in situ trace-element determinations in minerals. *Canadian Mineralogist* 30:1049–1064.

Jarosewich E. 1990. Chemical analyses of meteorites: A compilation of stony and iron meteorite analyses. *Meteoritics* 25:323–337.

Jenner G. A., Foley S. F., Jackson S. E., Green T. H., Fryer B. J., and Longerich H. P. 1993. Determination of partition coefficients for trace elements in high pressure-temperature experimental run products by laser ablation microprobe-inductively coupled plasma-mass spectrometry (LAM-ICP-MS). *Geochimica et Cosmochimica Acta* 58:5099–5103.

Kallemeyn G. W., Rubin A. E., Wang D., and Wasson J. T. 1989. Ordinary chondrites: Bulk compositions, classification, lithophile-element fractionations, and composition-petrographic type relationships. *Geochimica et Cosmochimica Acta* 53:2747–2767.

Kallemeyn G. W., Rubin A., and Wasson J. T. 1996. The compositional classification of chondrites: VII. The R chondrites group. *Geochimica et Cosmochimica Acta* 12:2243–2256.

Kessel R., Beckett J. R., and Stolper E. M. 2007. The thermal history of equilibrated ordinary chondrites and the relationship between textural maturity and temperature. *Geochimica et Cosmochimica Acta* 71:1855–1881.

Kurat G. 1969. The formation of chondrules and chondrites and some observations on chondrules from the Tieschitz meteorite. In: *Meteorite research*, edited by Millman P. M. Dordrecht: Reidel. pp. 185–190.

Kurat G., Brandstätter F., Pernicka E., and Kracher A. 1987. Bachmut (L6) chondrule J 2689: Metamorphism versus metasomatism. *Meteoritics* 22:A34–A35.

Laul J. C., Ganapathy R., Anders E., and Morgan J. W. 1973. Chemical fractionations in meteorites—VI. Accretion temperatures of H-, LL-, and E-chondrites, from abundance of volatile trace elements. *Geochimica et Cosmochimica Acta* 37:329–357.

Lodders K. and Fegley B. 1998. *The planetary scientist companion*. New York: Oxford University Press. 371 p.

McCanta M. C., Treiman A. H., Dyan M. D., Alexander C. M. O'D., Rumble D. III, and Essene E. J. 2008. The La Paz Icefield 04840 meteorite: Mineralogy, metamorphism, and origin of an amphibole- and biotite-bearing R chondrite. *Geochimica et Cosmochimica Acta* 72: 5757–5780.

McSween H. Y., Jr. and Labodka T. C. 1993. Oxidation during metamorphism of the ordinary chondrites. *Geochimica et Cosmochimica Acta* 57:1105–1114.

Mikouchi T., Ota K., Makishima J., Monkawa A., and Sugiyama K. 2007. Mineralogy and crystallography of LAP 04840: Implications for metamorphism at depth in the R chondrite parent body (abstract #1928). 38th Lunar and Planetary Science Conference. CD-ROM.

Pack A., Russell S. S., Shelley J. M. G., and Zuilen M. 2007. Geo- and cosmochemistry of the twin elements yttrium and holmium. *Geochimica et Cosmochimica Acta* 71: 4592–4608.

Rambaldi E. R., Wänke H., and Larimer J. W. 1979. Interelement refractory siderophile fractionation in ordinary chondrites. Proceedings, Lunar and Planetary Science Conference. pp. 997–1010.

Rambaldi E. R., Fredriksson B. J., and Fredriksson K. 1981. Primitive ultrafine matrix in ordinary chondrites. *Earth and Planetary Science Letters* 56:107–126.

Rubin A. E. 2010. Physical properties of chondrules in different chondrite groups: Implications for multiple melting events in dusty environments. *Geochimica et Cosmochimica Acta* 74:4807–4828.

Rubin A. E. and Kallemeyn G. W. 1989. Carlisle Lakes and Allan Hills 85151: Members of a new chondrite grouplet. *Geochimica et Cosmochimica Acta* 53:3035–3044.

Schulze H., Bischoff A., Palme H., Spettel B., Dreibus G., and Otto J. 1994. Mineralogy and chemistry of Rumuruti: The first meteorite fall of the new R chondrite group. *Meteoritics* 29:275–286.

Scott E. R. D. 2007. Chondrites and the protoplanetary disk. *Annual Review of Earth and Planetary Science* 35:577–620.

Sorby H. C. 1877. On the structure and origin of meteorites. *Nature* 15:495–498.

Van Schmus W. R. and Wood J. A. 1967. A chemical-petrographic classification for the chondritic meteorites. *Geochimica et Cosmochimica Acta* 31:747–765.

Warren P. H. 1997. The unequal host-phase density effect in electron probe defocused beam analysis: An easily correctable problem (abstract #1406). 28th Lunar and Planetary Science Conference. CD-ROM.

Weber H. W. and Schultz L. 1995. Noble gases in Rumuruti-group chondrites. *Meteoritics* 30:596.

Weisberg M. K., Prinz M., Kojima H., Yanai K., Clayton R. N., and Mayeda T. K. 1991. The Carlisle Lakes-type chondrites: A new grouplet with high $D^{17}O$ and evidence for nebular oxidation. *Geochimica et Cosmochimica Acta* 55:2657–2669.

Wlotzka F. 2005. Cr spinel and chromite as petrogenetic indicators in ordinary chondrites: Equilibration temperatures of petrologic types 3.7 to 6. *Meteoritics & Planetary Science* 40:1673–1702.